Research article

Wenhao Wu, Yu Yu*, Wei Liu and Xinliang Zhang

Fully integrated CMOS-compatible polarization analyzer

https://doi.org/10.1515/nanoph-2018-0205
Received November 26, 2018; revised January 15, 2019; accepted January 17, 2019

Abstract: Polarization measurement has been widely used in material characterization, medical diagnosis and remote sensing. However, existing commercial polarization analyzers are either bulky schemes or operate in non-real time. Recently, various polarization analyzers have been reported using metal metasurface structures, which require elaborate fabrication and additional detection devices. In this paper, a compact and fully integrated silicon polarization analyzer with a photonic crystal-like metastructure for polarization manipulation and four subsequent on-chip photodetectors for light-current conversion is proposed and demonstrated. The input polarization state can be retrieved instantly by calculating four output photocurrents. The proposed polarization analyzer is complementary metal oxide semiconductor-compatible, making it possible for mass production and easy integration with other silicon-based devices monolithically. Experimental verification is also performed for comparison with a commercial polarization analyzer, and deviations of the measured polarization angle are $<\pm 1.2\%$.

Keywords: polarimetry; Stokes measurement; polarization; silicon photonics.

1 Introduction

Polarization characterizes the vector nature of light in the plane perpendicular to the propagation direction. Polarized light plays an important role in many applications, such as microscopy, photography, communication and remote sensing [1–4]. Despite its superior capabilities and promising application prospects, the state of polarization (SOP) is normally hard to measure, as both the intensity and phase information of two orthogonal electromagnetic vectors should be specified simultaneously. A conventional polarization analyzer typically consists of a birefringent retardation plate and a linear polarizer, at least one of which should be rotatable around the propagation axis of the beam. The time-dependent intensity is then recorded with a detector and analyzed. Some other similar schemes using photoelastic modulators [5] or liquid crystal retarders [6] have also been reported. The performances of these polarization analyzers are limited by the rotation or modulation speed. Thus, they are inapplicable in situations where the polarization state varies rapidly. A different type of polarization analyzer avoids moving parts by splitting the beam up into several portions and handling diversely and simultaneously [7–9]. However, all the demonstrated ones were based on discrete and complex devices/components, lacking stability, compactness and reliability. Due to the compactness and stability that integrated devices can uniquely provide [10, 11], significant efforts have been made to develop integrated polarization analyzers. Recently, a metasurface, as a promising technique in integrated photonics [12], has been applied in characterizing polarization [13–22] because of its large design freedom and high efficiency in polarization handling. The working principle is similar to the splitting schemes mentioned above, and diverse distributions of nanoantenna arrays are set in different regions to manipulate the input SOP regionally and simultaneously. Although the metasurface schemes are ultracompact, their diffracted outputs cannot propagate on-chip and be processed by other silicon-based devices. Normally, an additional element, for example a charge-coupled device, is needed to collect the output light from the metasurface, which further complicates the measuring process and weakens the practicability. To tackle this issue, a splitting scheme fabricated on an InP platform was reported [23], however, it can only measure complete polarized light, as

***Corresponding author: Yu Yu,** Wuhan National Laboratory for Optoelectronics and School of Optical and Electronic Information, Huazhong University of Science and Technology, Wuhan 430074, China, e-mail: yuyu@mail.hust.edu.cn. https://orcid.org/0000-0002-8421-6794
Wenhao Wu, Wei Liu and Xinliang Zhang: Wuhan National Laboratory for Optoelectronics and School of Optical and Electronic Information, Huazhong University of Science and Technology, Wuhan 430074, China

only three dimensions of a Mueller matrix are considered. More recently, polarization analyzers based on the spin-orbit interaction [24] and polarization-frequency mapping [25] have been reported. Nevertheless, the former has a relatively low detection responsivity since only a little part of the input light can be coupled into the polarimeter, and the latter requires an additional waveform generator. Stokes vector receivers [26, 27] using two 3 dB-couplers, one 4 × 4 multimode-interference coupler and six photodetectors (PDs) are also reported, but they are designed for high-speed communication rather than the polarimetry. From these reported schemes, it can be found that fully integrated silicon-based polarization analyzers with a compact size and fast response speed are still in demand. In this paper, a complementary metal oxide semiconductor (CMOS)-compatible polarization analyzer is proposed and experimentally demonstrated.

A photonic-crystal (PhC)-like structure is adopted to achieve the polarization manipulation and an inverse design method is introduced to optimize the performance and decrease the footprint. Integrated high speed germanium (Ge) PDs are utilized to realize real time on-chip measurement. It is proved that arbitrary SOPs scattered on the Poincaré sphere can be retrieved by using the 4 × 2 transmission matrix of the device and the four output photocurrents. More importantly, the deviation of the transmission matrix, due to device imperfectness, can be partially calibrated by measuring input lights with known SOPs, which would greatly enlarge the fabrication tolerance of the proposed device. The size of the whole device is about 1 mm × 0.3 mm, which is much smaller than the previous scheme [23, 27]. The mature edge coupling technique is adopted to enhance the responsivity. The proposed polarization analyzer is characterized using a commercial product for comparison and the deviation of the measured polarization angle is <±1.2%. More specifically, the deviations of azimuth, ellipticity angle and degree of polarization (DOP) are –2.08° ~ 2.15°, –1.1° ~ 1.3°, and –0.07 ~ 0.07, respectively.

2 Device design

The schematic of the device demonstrated in this work is shown in Figure 1. The external light is firstly coupled into the photonic integrated circuit through a spot-size converter, and then split into two transverse electric (TE) signals through a polarization splitter-rotator (PSR). One of the signals comes from the TE component of the input and the other originates from the transverse magnetic (TM) component. After transmitting through the polarization hybrid unit (PHU), the two signals are hybridized and split into four portions, which are finally detected by four PDs. It is worth noting that the PHU possesses symmetry along the Z-axis and is specially designed so that output port O1 (O4) only has a signal from the input port IN1 (IN2), showing intensity information of the input SOP, while ports O2 and O3 both have signals from IN1 and IN2 as a hybrid coupler, indicating phase information of the input SOP. Thus, the input SOP can be retrieved from the four output signals. The working principle is proved by using Jones calculus. Here, we assume an ideal case where excess loss, polarization dependence loss and fabrication imperfection are ignored. The input light can be described as a Jones vector $\boldsymbol{E} = [E_x, E_y \exp(j\theta)]^T$, where '$E_x$' and '$E_y$' are the amplitudes of the electric field components in the horizontal (x) and vertical (y) directions, and 'θ' is the phase difference between the two components. $\boldsymbol{J}_{PSR}$ and $\boldsymbol{J}_{PHU}$ are the transmission matrices of the PSR and PHU, and their product $\boldsymbol{J}_{PA}$ is the transmission matrix of the polarization

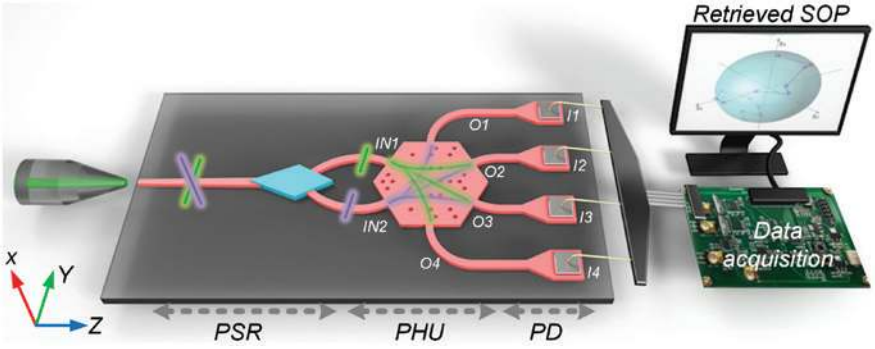

Figure 1: Schematic of the polarization analyzer. It consists of a polarization splitter-rotator (PSR), a polarization hybrid unit (PHU) and four photodetectors (PDs). Four Output electric signals I1–I4 are collected by the data acquisition unit and analyzed to retrieve the input state of polarization (SOP).
The green and purple lines represent two orthogonal polarization components.

analyzer. The output of the polarization analyzer $\boldsymbol{O}_{PA}$ can be described as $\boldsymbol{O}_{PA}=\boldsymbol{J}_{PA}\cdot\boldsymbol{E}=\boldsymbol{J}_{PHU}\cdot\boldsymbol{J}_{PSR}\cdot\boldsymbol{E}$

$$=\begin{bmatrix} 0 & A\exp(j\varphi_1) \\ C\exp(j\varphi_3) & B\exp(j\varphi_2) \\ B\exp(j\varphi_2) & C\exp(j\varphi_3) \\ A\exp(j\varphi_1) & 0 \end{bmatrix}\cdot\begin{bmatrix} 1 & 0 \\ 0 & \exp(j\psi) \end{bmatrix}\cdot\boldsymbol{E}, \quad (1)$$

where 'ψ' is the phase difference between the two outputs of the PSR and 'A', 'B', 'C', 'φ_1', 'φ_2' and 'φ_3' are the splitting ratios and phase shifts for the different transmission paths in the PHU, as shown in Figure 2A. Ideally, $A^2=B^2=C^2=1/3$. In this scenario, the measured photocurrent I_i of the i-th PD can be described as:

$$\begin{aligned} I_1 &= RA^2\left|E_y\right|^2 \\ I_2 &= R\left(C^2\left|E_x\right|^2+B^2\left|E_y\right|^2+2CB\left|E_xE_y\right|\cos(\varphi_2+\psi-\varphi_3+\theta)\right) \\ I_3 &= R\left(B^2\left|E_x\right|^2+C^2\left|E_y\right|^2+2CB\left|E_xE_y\right|\cos(\varphi_3+\psi-\varphi_2+\theta)\right) \\ I_4 &= RA^2\left|E_x\right|^2 \end{aligned}, \quad (2)$$

where R represents the responsivity of PDs. According to the definition of Stokes vector provided in [28], the Stokes parameters can be represented by using the four measured photocurrents as:

$$\begin{aligned} S_0 &= 1 \\ S_1 &= (I_4-I_1)/(I_4+I_1) \\ S_2 &= [m_1\sin(\varphi_3+\psi-\varphi_2)-m_2\sin(\varphi_2+\psi-\varphi_3)]/M \\ S_3 &= \left[m_1\cos(\varphi_3+\psi-\varphi_2)-m_2\cos(\varphi_2+\psi-\varphi_3)\right]/M \end{aligned}, \quad (3)$$

where $m_1=I_2-I_1-I_4$, $m_2=I_2-I_1-I_4$ and $M=\sin(2\varphi_3-2\varphi_2)(I_4+I_1)$.

In practical situations, the transmission matrix of the polarization analyzer may deviate from Eq. (1). Deviations of zero terms indicate crosstalk, which makes intensities of TE and TM components obtained from O1 and O4 of the PHU relate to their relative phase. Because the relative phase is unknown for an inputting SOP, this crosstalk cannot be calibrated and will degrade the measuring accuracy. By contrast, deviations of nonzero terms indicate propagation loss, imperfect splitting ratio and phase shift, which can be calibrated by measuring a series of known SOPs. As an example, the coupling loss and transmission loss differences between TE and TM modes can be calibrated comprehensively by pre-characterizing the outputs of 0° and 90° polarized input light.

The proposed device is designed on the widely used commercial silicon-on-insulator (SOI) platform with a 220 nm top Si layer and 3 μm SiO_2 cladding.

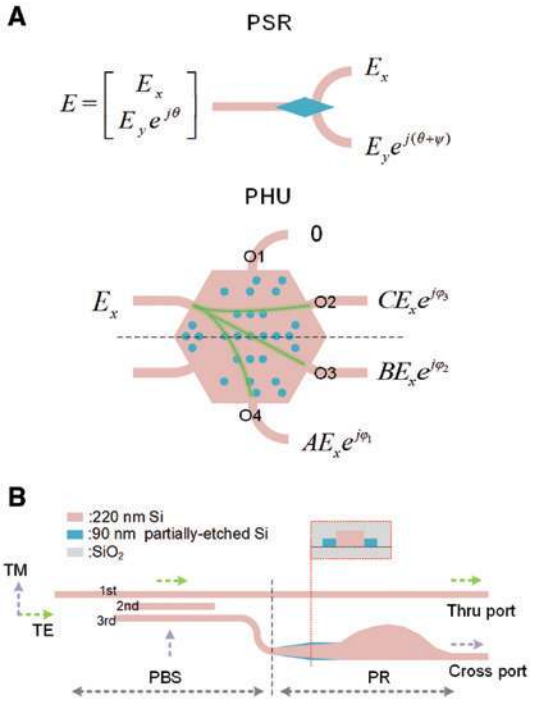

Figure 2: Working principles of the PSR and PHU.
(A) The transmission characteristics of the polarization splitter-rotator (PSR) and the polarization hybrid unit (PHU). Only E_x is considered in the PHU because of the symmetry. (B) The schematic and the working principle of the PSR. Thru = through.

The PSR consists of a polarization beam splitter [29] and a polarization rotator [30] with detailed structures shown in Figure 2B. The fundamental TE (TE_0) signal from the input port transmits straight along the waveguide and maintains TE_0 at the through port. For the fundamental TM (TM_0) signal, it will be coupled to the third waveguide of the polarization beam splitter and then converted into the first order TE (TE_1) mode through a bi-level taper, which has a 90 nm slab. Finally, the TE_1 mode is further transformed into TE_0 using a mode-order convertor [31] based on cascaded tapers.

The PHU possesses symmetry and has two inputs and four special outputs. It is straightforward to design a structure with a hexagonal outline as a representative. A PhC-like metastructure is introduced to raise freedom of design, and an inverse design method using direct binary search [32] is adopted to achieve an optimal structure. Circle holes are arranged in a certain pattern in the symmetrical hexagonal structure with a side length of 3.36 μm. As shown in Figure 3A, the hole radius is 150 nm to meet the fabrication criterion, and the center distance between every two adjacent holes is set as 560 nm to ensure separation after fabrication. These holes have a binary state of the dielectric property: 220 nm or 90 nm thick silicon. A 90 nm thickness is chosen to decrease the fabrication

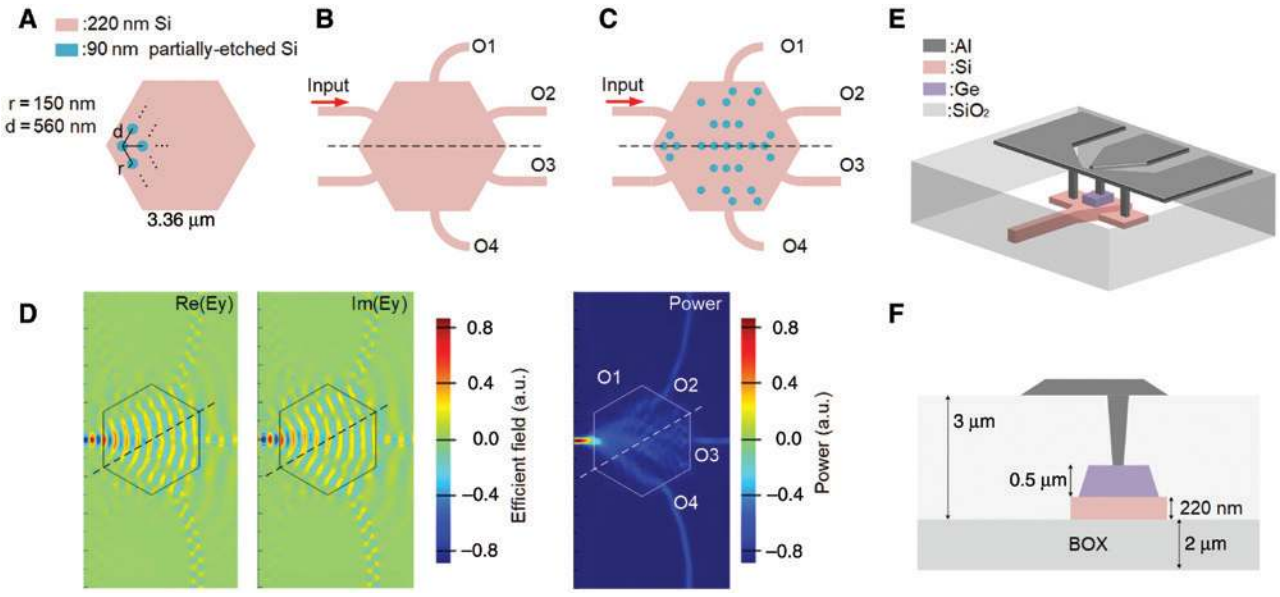

Figure 3: Design process of the PHU and layout of the PD.
(A) The illustration of the holes' size and distribution rules. (B) The initial pattern of the simulation for the polarization hybrid unit (PHU). (C) The optimized pattern of the simulation for the PHU. (D) The real/imaginary parts of the simulated electric field and power distributions of the optimized PHU at 1550 nm. (E) 3D schematic and (F) cross section of the Ge photodetector. BOX = buried oxide.

difficulty and simplify the fabrication process, since the slab waveguide in the PSR has the same thickness.

Due to the symmetrical structure of the PHU, only one input should be considered in the design process, and the 3D finite-difference time-domain method is applied to simulate the PHU at the wavelength of 1550 nm. Firstly, all of the holes are set as 220 nm thick to initialize the optimization process, as shown in Figure 3B. One hole state is switched in each iteration, and whether the state should be 220 or 90 nm thick silicon is determined by a figure of merit (FOM), which is defined as an expression of the root-mean-square deviation of four outputs:

$$\mathrm{FOM}_i = a\frac{\sqrt{E_{1,i}^2 + E_{5,i}^2}}{2} + (1-a)\frac{\sqrt{\sum_{j=2}^{4}(E_{j,i} - 1/3)^2}}{3} \quad (4)$$

where FOM_i is the FOM after the i-th iteration, and $E_{j,i}$ is the transmission efficiency of the j-th output waveguide in the i-th iteration. In this simulation, the fifth output, which is not labeled in Figure 3, is the other input of the PHU. A weight coefficient a is set as 0.8 to preferentially consider $E_{1,i}$ and reduce the crosstalk, since it cannot be calibrated. If $\mathrm{FOM}_i < \mathrm{FOM}_{i-1}$, the i-th switch of state can be preserved, otherwise the i-th hole returns to the original state. When all the hole states have been switched, it is a round of iteration. After six rounds of iteration, the FOM becomes convergent, and the layout of the PHU is shown in Figure 3C. Figure 3D illustrates the electric field and power distribution in the PHU. The final transmission efficiencies of the five outputs T1 ~ T5 are, respectively, 0.003, 0.1, 0.21, 0.15 and 0.002. Crosstalk of the PHU, defined as –10 lg (T4/T1), is about –17 dB, and it determines the measuring accuracy and bandwidth of the PHU. In this paper, the bandwidth is defined as the wavelength range during which the crosstalk is lower than –16 dB. Under this circumstance, the bandwidth of the PHU is ~60 nm at the central wavelength of 1550 nm. Effective ways to decrease the crosstalk are to further optimize the hole number, radius and center distance, to further raise the freedom of design, at the cost of increasing fabrication difficulty.

For the detection part, the typical waveguide coupled Ge PDs [33], shown in Figure 3E, are used to transform the optical signals into electrical ones. The input light is first transmitted to a shallow etched silicon area through a taper and then absorbed by the Ge grown on the silicon. The width, length, and height of the Ge region are 5 μm, 10 μm, and 0.5 μm, respectively. The transformed photocurrent can be collected through the aluminum electrode grown on the Ge region. The cross section of the PD is shown in Figure 3F.

3 Results

Microscope images of the fabricated polarization analyzer and the PHU are shown in Figure 4. Before testing the whole device, first, a reference PSR is characterized

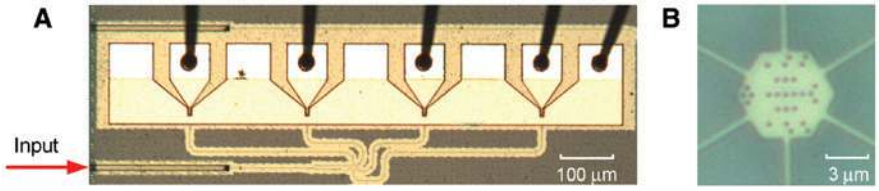

Figure 4: Fabricated polarization analyzer.
Microscope images of (A) the whole device and (B) the polarization hybrid unit (PHU). The wire bonding technique is used for electrical connection between the on-chip electrode pads and the printed circuit board pads.

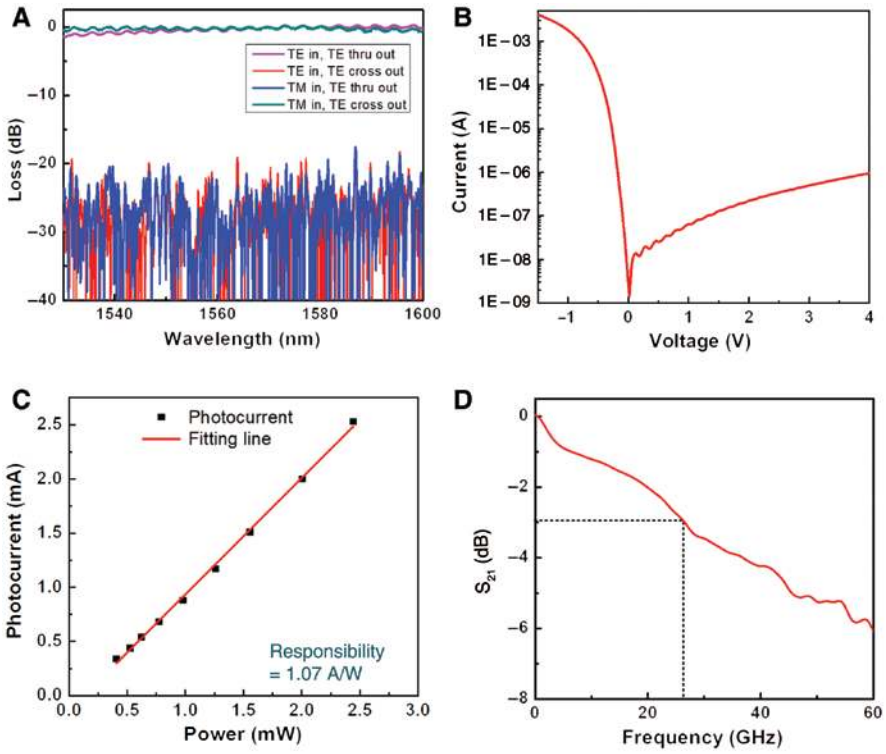

Figure 5: Measured performances of the PSR and PD.
(A) Measured loss and crosstalk of the polarization splitter-rotator (PSR) for transverse electric (TE) and transverse magnetic (TM) input; (B) measured dark current; (C) responsivity and (D) S_{21} curve of the Ge photodetector when the reverse biased voltage is 3 V.

through the method demonstrated in [32]. Figure 5A shows the measured loss and crosstalk for the TE/TM mode. The TE-TE insertion loss is lower than 1 dB over the wavelength range of 1530–1600 nm, while the crosstalk is lower than –20 dB. As for the TM mode, the TM-TE polarization conversion loss and the crosstalk are lower than 0.5 and –19 dB, respectively. A reference Ge PD is also tested to acquire the dark current, responsivity and bandwidth. As shown in Figures 5B and 5C, the dark current at a voltage of 3 V is 0.3 μA and the responsivity is 1.07 A/W. Figure 5D shows that the 3-dB bandwidth is about 26 GHz according to the measured S_{21} curve. Although a PD with a small bandwidth is capable of polarization measurement, the proposed device can also monitor the input high-speed signal, for example eye diagrams, while measuring the polarization state, thanks to the large bandwidth.

Next, the fabricated polarization analyzer is fully characterized by using the experimental setup shown in Figure 6. A continuous-wave light at 1550 nm from a tunable laser is first sent through a rotatable spatial polarizer; it is then separated to two paths by a 20:80 beam splitter. The 80% part is coupled into the proposed polarization analyzer by using a non-polarization-maintaining (non-PM) fiber, while the 20% part is linked to a commercial bench-top polarization analyzer (Santec PAM-320). Polarization controllers (PC2, PC3 and PC4) are carefully calibrated to compensate the SOP variations through the non-PM fibers, ensuring that the input SOPs of the two polarization analyzers are identical. In this case, the

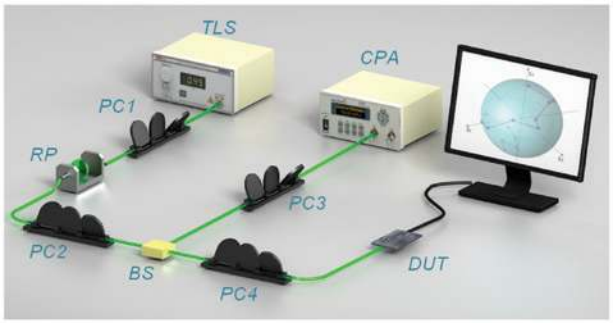

Figure 6: Experiment setup for characterization of the proposed polarization analyzer.
BS, beam splitter; CPA, commercial polarization analyzer; DUT, device under test; RP, rotatable polarizer; TLS, tunable laser source.

on-chip polarization analyzer can be characterized by comparing with the commercial one.

In practical situations, the proposed polarization analyzer needs to be pre-calibrated to derive the transmission matrix of the fabricated device $\boldsymbol{J}_{\mathrm{PA}}^{*}$. One common method is sending a series of light with known SOPs and recording the photocurrent of each PD. More specifically, a series of linear polarized lights were used by rotating the spatial polarizer to different angles.

The experimental procedure is demonstrated below. First, the linear polarized case is considered. We rotate the spatial polarizer from 0° to 180° with a step of 10° to generate linear polarization light and adjust the PC1 to ensure the input power is largest. Meanwhile, the output photocurrents from the on-chip polarization analyzer and the Stokes parameters measured by the commercial one are recorded. Then, we changed the state of PC2 to investigate the elliptic-polarized input case. After calculation, the performance of the proposed polarization analyzer can be characterized by comparing the deduced Stokes parameters with those measured by the commercial one.

The derived actual transmission matrix of the whole structure $\boldsymbol{J}_{\mathrm{PA}}^{*}$ is (see derivation method in Supplementary Material):

$$\boldsymbol{J}_{\mathrm{PA}}^{*}=\begin{bmatrix} 0 & 0.96 \\ 1.55 & 1.35\mathrm{e}^{\mathrm{j}(0.257\pi)} \\ 1.46 & 1.60\mathrm{e}^{\mathrm{j}(0.838\pi)} \\ 1 & 0 \end{bmatrix}, \tag{5}$$

By using the measured photocurrents $\mathrm{I}_1 \sim \mathrm{I}_4$ and the derived transmission matrix $\boldsymbol{J}_{\mathrm{PA}}^{*}$, any arbitrary SOP could be retrieved. Figure 7A depicts the SOPs retrieved from the on-chip polarization analyzer and measured by the commercial one in the form of the Poincaré sphere with linear polarization inputs. The retrieved SOP travels along the

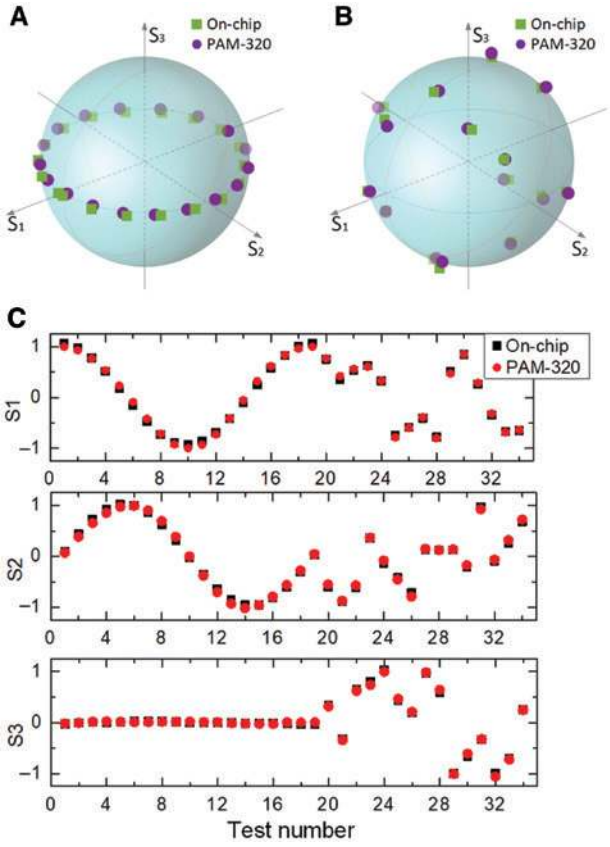

Figure 7: Retrieved SOPs of the proposed polarization analyzer and the commercial one.
The measured Stokes parameters from the two polarization analyzers with (A) linear-polarized and (B) elliptic-polarized inputs. (C) The measured Stokes parameters for various polarization states. The working wavelength is 1550 nm.

equator of the Poincaré sphere in agreement with theory. Figure 7B shows the measured SOPs from the two polarization analyzers with elliptical polarization inputs, and excellent agreement between these two sets of results is observed. For quantitative comparison, measured Stokes parameters for various polarization states are shown in Figure 7C, and deviations of S1, S2 and S3 between the two polarization analyzers are −0.07 ~ 0.06, −0.05 ~ 0.07 and −0.05 ~ 0.06, respectively. Figure 8 indicates that the deviations of azimuth, ellipticity angle and DOP are –2.08° ~ 2.15°, –1.1° ~ 1.3°, and −0.07 ~ 0.07, respectively. Compared with the polarization analyzers in [21] and [24] with angle deviations of 5.57° and 10°, respectively, the proposed device shows great performance in terms of measuring accuracy. It should be noted that the actual accuracy of the on-chip polarization analyzer may be better than the tested results, since the utilized commercial product has a ±0.45° polarization angle deviation according to the datasheet. Besides, the instability of the coupling between fiber and chip also degrades the tested accuracy, which can be alleviated by packaging.

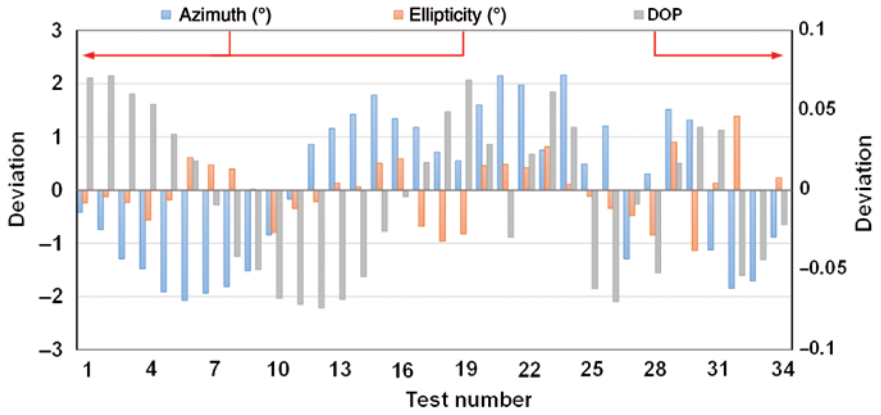

Figure 8: Deviations of azimuth, ellipticity angle and degree of polarization (DOP) between the measured results from the proposed polarization analyzer and the commercial one.

Although only complete polarized light is experimentally tested, it should be noted that partially polarized light which contains some natural light can also be retrieved by the proposed device. It can be easily verified by replacing $|E_x|^2$ and $|E_y|^2$ with $(|E_x|^2+0.5F)$ and $(|E_y|^2+0.5F)$ in Eqs. (2) and (3), where F is the intensity of the natural light.

4 Conclusion

In conclusion, we have demonstrated a fully integrated CMOS-compatible polarization analyzer, for the first time to our best knowledge. A PhC-like metastructure is introduced to reduce the footprint, and four high-speed Ge PDs are integrated to form a complete analyzer. The working principle of the device is first elucidated, and then a proof-of-concept device is fabricated on an SOI wafer. The input SOPs can be retrieved in real time by calculating the four output photocurrents. Experimental results show a good and actual polarization measurement, by comparing with a commercial product. The proposed CMOS-compatible polarization analyzer can be integrated with other commonly used silicon-based devices, showing great potential for on-line polarization measurement and monitoring in large-scale silicon photonic systems.

5 Methods

The proposed polarization analyzer was fabricated on an SOI wafer with a 220 nm top Si layer and 3 μm SiO_2 cladding. The waveguide structure was patterned via deep ultraviolet lithography and inductively coupled plasma etching. The polarization analyzer was tested using a tunable laser (Alnair Labs TLG-200). To increase the coupling efficiency between the fiber and chip, spot size converters are introduced via inversely tapering silicon waveguides to 180 nm width tips at the chip edge. The coupling loss is 2 dB using single-mode lensed fibers.

The derivation method for the transmission matrix of the fabricated polarization analyzer $\boldsymbol{J}^*_{\mathrm{PA}}$. is shown in Supplementary Material

Acknowledgments: The authors acknowledge funding from the National Natural Science Foundation of China (Funder Id: http://dx.doi.org/10.13039/501100001809, Grant No. 61775073 and 61475050), the New Century Excellent Talent Project in Ministry of Education of China (Funder Id: http://dx.doi.org/10.13039/501100004602, NCET-13-0240).

References

[1] Arvidson RE. Photometry and polarization in remote sensing. Eos, Transactions American Geophysical Union 1986;67:122–2.
[2] Deuzé JL, Bréon FM, Devaux C, et al. Remote sensing of aerosols over land surfaces from POLDER-ADEOS-1 polarized measurements. J Geophys Res Atmos 2001;106:4913–26.
[3] Andrews MR, Mitra PP, deCarvalho R. Tripling the capacity of wireless communications using electromagnetic polarization. Nature 2001;409:316–8.
[4] van Uden RGH, Amezcua Correa R, Antonio Lopez E, et al. Ultra-high-density spatial division multiplexing with a few-mode multicore fibre. Nature Photon 2014;8:865–70.
[5] Alali S, Yang T, Vitkin IA. Rapid time-gated polarimetric Stokes imaging using photoelastic modulators. Opt Lett 2013;38:2997–3000.
[6] De Martino A, Kim Y-K, Garcia-Caurel E, Laude B, Drévillon B. Optimized Mueller polarimeter with liquid crystals. Opt Lett 2003;28:616–8.

[7] Morel O, Seulin R, Fofi D. Handy method to calibrate division-of-amplitude polarimeters for the first three Stokes parameters. Opt Express 2016;24:13634–46.
[8] Hsu WL, Myhre G, Balakrishnan K, Brock N, Ibn-Elhaj M, Pau S. Full-Stokes imaging polarimeter using an array of elliptical polarizer. Opt Express 2014;22:3063–74.
[9] Mu T, Zhang C, Li Q, Liang R. Error analysis of single-snapshot full-Stokes division-of-aperture imaging polarimeters. Opt Express 2015;23:10822–35.
[10] Cheng Q, Bahadori M, Glick M, Rumley S, Bergman K. Recent advances in optical technologies for data centers: a review. Optica 2018;5:1354–70.
[11] Atabaki AH, Moazeni S, Pavanello F, et al. Integrating photonics with silicon nanoelectronics for the next generation of systems on a chip. Nature 2018;556:349–54.
[12] Arbabi A, Horie Y, Bagheri M, Faraon A. Dielectric metasurfaces for complete control of phase and polarization with subwavelength spatial resolution and high transmission. Nat Nanotechnol 2015;10:937–43.
[13] Afshinmanesh F, White Justin S, Cai W, Brongersma Mark L. "Measurement of the polarization state of light using an integrated plasmonic polarimeter," in *Nanophotonics* vol. 1, ed, 2012, p. 125.
[14] Xie Y-B, Liu Z-Y, Wang Q-J, Zhu Y-Y, Zhang X-J. Miniature polarization analyzer based on surface plasmon polaritons. Appl Phys Lett 2014;105:101107.
[15] Pors A, Nielsen MG, Bozhevolnyi SI. Plasmonic metagratings for simultaneous determination of Stokes parameters. Optica 2015;2:716–23.
[16] Balthasar Mueller JP, Leosson K, Capasso F. Ultracompact metasurface in-line polarimeter. Optica 2016;3:42–7.
[17] Maguid E, Yulevich I, Veksler D, Kleiner V, Brongersma ML, Hasman E. Photonic spin-controlled multifunctional shared-aperture antenna array. Science 2016;352:1202–6.
[18] Chen WT, Török P, Foreman MR, et al. Integrated plasmonic metasurfaces for spectropolarimetry. Nanotechnology 2016;27:224002.
[19] Ding F, Pors A, Chen Y, Zenin VA, Bozhevolnyi SI. Beam-size-invariant spectropolarimeters using gap-plasmon metasurfaces. ACS Photonics 2017;4:943–9.
[20] Maguid E, Yulevich I, Yannai M, Kleiner V, Brongersma ML, Hasman E. Multifunctional interleaved geometric-phase dielectric metasurfaces. Light-Sci Appl 2017;6:e17027.
[21] Lee K, Yun H, Mun SE, Lee GY, Sung J, Lee B. Ultracompact broadband plasmonic polarimeter. Laser Photonics Rev 2018;12:1700297.
[22] Rubin NA, Zaidi A, Juhl M, et al. Polarization state generation and measurement with a single metasurface. Opt Express 2018;26:21455–78.
[23] Ghosh S, Kawabata Y, Tanemura T, Nakano Y. Polarization-analyzing circuit on InP for integrated Stokes vector receiver. Opt Express 2017;25:12303–10.
[24] Espinosa-Soria A, Rodríguez-Fortuño FJ, Griol A, Martínez A. On-chip optimal Stokes nanopolarimetry based on spin–orbit interaction of light. Nano Lett 2017;17:3139–44.
[25] Zhou H, Yan S, Wei Y, et al. Silicon-based polarization analyzer by polarization-frequency mapping. APL Photonics 2018;3:106105.
[26] Che D, Li A, Chen X, Hu Q, Wang Y, Shieh W. Stokes vector direct detection for short-reach optical communication. Opt Lett 2014;39:3110–3.
[27] Dong P, Chen X, Kim K, Chandrasekhar S, Chen Y-K, Sinsky JH. 128-Gb/s 100-km transmission with direct detection using silicon photonic Stokes vector receiver and I/Q modulator. Opt Exp 2016;24:14208–14.
[28] Milione G, Sztul HI, Nolan DA, Alfano RR. Higher-order Poincaré sphere, stokes parameters, and the angular momentum of light. Phys Rev Lett 2011;107:053601.
[29] Kim DW, Lee MH, Kim Y, Kim KH. Planar-type polarization beam splitter based on a bridged silicon waveguide coupler. Opt Express 2015;23:998–1004.
[30] Chen D, Xiao X, Wang L, Liu W, Yang Q, Yu S. Highly efficient silicon optical polarization rotators based on mode order conversions. Opt Lett 2016;41:1070–3.
[31] Chen D, Xiao X, Wang L, Yu Y, Liu W, Yang Q. Low-loss and fabrication tolerant silicon mode-order converters based on novel compact tapers. Opt Express 2015;23:11152–9.
[32] Shen B, Wang P, Polson R, Menon R. An integrated-nanophotonics polarization beamsplitter with $2.4 \times 2.4\ \mu m^2$ footprint. Nat Photonics 2015;9:378–82.
[33] Chen G, Yu Y, Xiao X, Zhang X. High speed and high power polarization insensitive germanium photodetector with lumped structure. Opt Express 2016;24:10030–9.

Supplementary Material: The online version of this article offers supplementary material (https://doi.org/10.1515/nanoph-2018-0205).